

Estimating the Coupling between Variations in the Atlantic Multidecadal Oscillation and the El Niño/Southern Oscillation

I. I. Mokhov^a and D. A. Smirnov^{b, c}

^a *Obukhov Institute of Atmospheric Physics, Russian Academy of Sciences, Pyzhevskii per. 3, Moscow, 119017 Russia*
e-mail: mokhov@ifaran.ru

^b *Kotel'nikov Institute of Radio Engineering and Electronics, Saratov Branch, Russian Academy of Sciences, ul. Zelenaya 38, Saratov, 410019 Russia*

^c *Institute of Applied Physics, Russian Academy of Sciences, ul. Ul'yanova 46, Nizhny Novgorod, 603950 Russia*
e-mail: smirnovda@yandex.ru

Received August 11, 2014; in final form, October 28, 2014

Abstract—On the basis of monthly mean data obtained over a period of 1870–2013, relations between the Atlantic Multidecadal Oscillation (AMO) and the El Niño/Southern Oscillation (ENSO) have been studied using the Granger causality analysis and estimates of long-term effects. A bidirectional relationship has been revealed in the dynamics of these processes; moreover, over the entire period as a whole, the ENSO influence on the AMO was significantly stronger than the AMO influence on the ENSO. However, a more detailed analysis has revealed the variable character of this relationship: the ENSO influence on the AMO was stronger at the beginning of the period under study, while, in recent years, the reverse influence and its increase have become more significant against the background of a decrease in the ENSO influence on the AMO.

Keywords: climate variability, quasi-cyclic processes, El Niño/Southern Oscillation, Atlantic multidecadal oscillation, cause–effect relations

DOI: 10.1134/S0001433815050084

1. INTRODUCTION

Significant global and regional climatic processes are associated with quasi-cyclic phenomena, such as the El Niño/Southern Oscillation (ENSO) and the Atlantic Multidecadal Oscillation (AMO) [1, 2–9]. Determining the interrelation between global climate variations over the past 150 years and quasi-cyclic processes like the ENSO, the AMO, and the Pacific Decadal Oscillation, which significantly affect both global and regional climate changes with periods of a few years to a few decades, is one of the key problems of climate studies. Justified quantitative estimates and a reliable understanding of the interaction between key large-scale processes are necessary.

The ENSO quasi-cyclic processes are characterized by surface temperature anomalies in the Pacific equatorial latitudes with a periodicity of 2 to 8 years (on average, about 4–5 years). In addition, noticeable multidecadal variations in the ENSO phenomena manifest themselves. The AMO manifests itself in North Atlantic surface-temperature fluctuations with a periodicity of about 60 years. Moreover, noticeable decadal and intradecadal variations in the AMO manifest themselves. The results of a cross-wavelet analysis of different ENSO and AMO indices point to a significant coherence and both longer term (multidecadal and decadal) and shorter term (interannual and intra-

annual) variations in these quasi-cyclic processes [4, 6, 16, 17, 23]. It should be noted that, along with the time intervals of a more statistically significant coherence between the ENSO and the AMO, intervals with statistically insignificant coherence are also noted.

In this work the interdependence of ENSO and AMO variations is analyzed using empirical data obtained over the past 150 years and the construction of autoregressive models on the basis of which different characteristics of this relationship—relatively short-term and longer term effects—are determined. Such short-term effects are characterized by Granger causality estimates (prediction improvements of empirical models) [10–13], which are more often used in analyzing climatic data [14–23]. To develop a general approach [15, 16], it was suggested that long-term effects be characterized by changes in the process variance under changes in coupling parameters and noise sources in an empirical model.

2. DATA USED

Monthly means (<http://www.esrl.noaa.gov/>) for the anomalies of the ENSO and AMO indices I_E and I_A , respectively, for a period of 1870–2013 were used in our analysis. The temperature of the Pacific surface in the subequatorial region Niño 3.4 (5° N–5° S, 170°–

120° W) was used as index I_E , and the sea surface temperature in the North Atlantic region (0°–70° N) was used as index I_A . The time-series data under analysis with eliminated annual cycle are given in Fig. 1.

3. METHODS FOR ESTIMATING BOTH SHORT- AND LONG-TERM RELATIONS

Let us assume that we have a time series of two processes $\{x_k(t)\}$, $t = 1, 2, \dots, N$, $k = 1, 2$, where x_k is variables and N is the length of the series. It is necessary to find out whether process x_1 influences process x_2 (effect $1 \rightarrow 2$) and whether process x_2 influences process x_1 (effect $2 \rightarrow 1$) with quantitative estimates of these influences.

3.1. Estimating Short-Term Relation

Granger causality estimates are based on the construction of empirical models and on calculations of errors of the one-step forward (short-term) prediction of one process with and without consideration for the other process [10–13]. Then, in estimating linearly, one can use a conventional procedure (see, for example, [21, 22]). At first, the individual autoregressive (AR) models are constructed:

$$x_k(t) = A_{k,0} + \sum_{i=1}^{d_k} A_{k,i} x_k(t-i) + \xi_k(t), \quad k = 1, 2, \quad (1)$$

where d_k is the model order and ξ_k is white noise. Here and below, the following symbols are used: $\sum_k^2 = \sum_{t=d_{\max}+1}^N \left(x_k(t) - A_{k,0} - \sum_{i=1}^{d_k} A_{k,i} x_k(t-i) \right)^2$ is the sum of squared residual errors of the model, d_{\max} is the maximum test-model order, and \mathbf{A}_k is the vector of the coefficients $A_{k,i}$. The vector \mathbf{A}_k is estimated using the method of least squares, i.e., $\hat{\mathbf{A}}_k = \arg \min_{\mathbf{A}_k} \sum_k^2$.

When $s_k^2 = \min_{\mathbf{A}_k} \sum_k^2$ is introduced, the estimate of the variance of noise ξ_k takes the form $\hat{\sigma}_k^2 = s_k^2 / (N - d_{\max})$. In order to select d_k , the Schwartz information criterion [26] is used: d_k varies from zero to d_{\max} and is chosen from the condition of minimization of $S_k = \frac{(N - d_{\max})}{2} \ln \hat{\sigma}_k^2 + \frac{d_k + 1}{2} \ln(N - d_{\max})$. If d_k is found, the joint model is constructed:

$$x_k(t) = a_{k,0} + \sum_{i=1}^{d_k} a_{k,i} x_k(t-i) + \sum_{j=1}^{d_{j \rightarrow k}} b_{k,i} x_j(t-i) + \eta_k(t), \quad k, j = 1, 2, \quad j \neq k, \quad (2)$$

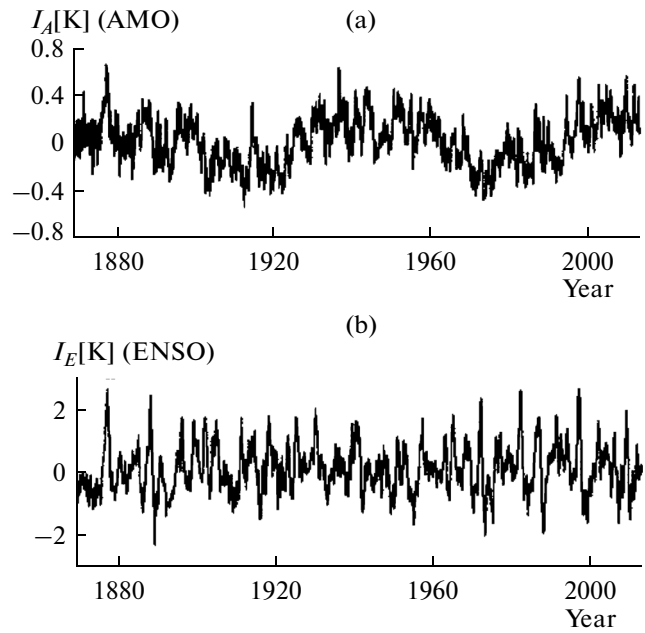


Fig. 1. (a) AMO and (b) ENSO indices with eliminated annual variations.

where $d_{j \rightarrow k}$ is the number of x_j , values taken into account and η_k is white noise. The coefficients of model (2) are also determined using the method of least squares. If the variance of its residual errors is represented by $\hat{\sigma}_{k|j}^2$, then the normalized value of prediction improvement $PI_{j \rightarrow k} = (\hat{\sigma}_k^2 - \hat{\sigma}_{k|j}^2) / \hat{\sigma}_k^2$ characterizes the influence $j \rightarrow k$.

In order to estimate the statistical significance of the inference about the difference of $PI_{j \rightarrow k}$ from zero, the Fisher F -test [27] is used, which, at a given $d_{j \rightarrow k}$, characterizes the significance level of derived p (probability of random error). Since the testing is conducted at different test dimensionalities (multiple) up to the current $d_{j \rightarrow k}$, the total significance level proves worse (i.e., higher) than the pointwise level of p . The often-used Bonferroni correction [16, 17, 21, 22] is determined by multiplying p by the number of conducted tests for $d_{j \rightarrow k}$. In order to select $d_{j \rightarrow k}$, $d_{j \rightarrow k} p$ is minimized (below p_{\min}). If p_{\min} is lower than some small value (0.05 or 0.1), it is assumed that the prediction improvement is nonzero and the $j \rightarrow k$ effect is present; however, the latter is not always strongly valid [28–31]. The Schwarz criterion in selecting $d_{j \rightarrow k}$ proves stricter and it often yields the zero optimal value of $d_{j \rightarrow k}$, even if, at nonzero values of $d_{j \rightarrow k}$, the values of p_{\min} are small (of an order of 0.01). Then both results obtained in selecting d_k on the basis of the Schwartz criterion and $d_{j \rightarrow k}$ on the basis of the Fisher criterion are given. The trial values of d_k and $d_{j \rightarrow k}$ vary

within such a range that the number of coefficients in any used AR model is significantly smaller than the length of the data series under analysis. First, estimates are obtained for the entire 1870–2013 interval and then an analysis is made using sliding windows. In analyzing the whole data series or its significant part (window 60 years in length), it is assumed that $d_{\max} = 12$. At window lengths of 10, 20, and 30 years, it is assumed that $d_{\max} = 6$ so that the total number of coefficients in each equation of the joint model remains always smaller than \sqrt{N} .

Searching for model (2) according to the least rms prediction error must simultaneously provide the delta-correlation of the residual errors of the model (i.e., the correspondence of their properties to the requirement of the white noises ξ_k and η_k in AR models) at its sufficient dimensionality [10, 11, 26]. This condition was satisfied for all optimal models, which was verified according to estimates of the correlation functions of residual errors.

Nonlinear estimates are similarly obtained; only nonlinear (instead of linear) functions are used in the right-hand sides of AR equations. In this work, low-order polynomials are used, because the volume of data is limited and the number of AR-model coefficients rapidly increases with an increase in the order of polynomial.

3.2. Estimating Long-Term Relation

The Granger causality characterizes errors of the one-step forward prediction, i.e., to what extent the presence of one process (x) affects the spread in the values of the other (y) at the next point of time when the state of y is fixed at the moment. This reflects the short-term effect of x on y . It is also important to diagnose what long-term variations in one process may result from variations not only in the initial state of the other process, but also in its parameters or in coupling parameters. In [24, 25], this was estimated from an analysis of the dynamics of AR model (2) constructed under the assumption that this model adequately reflects the functioning of the processes even under variations in the corresponding parameters. Namely, the effect of parameter variations on trends was estimated, since variations in the global surface air temperature were analyzed. In this work, when estimating the effects of the long-term coupling, we (developing the approach described in [24, 25]) analyzed the variance of the processes (i.e., the total fluctuation power within a time interval exceeding the characteristic time scales of the processes) and its change under certain hypothetical variations in the AR-model parameters.

The noise in AR model (2) was assumed Gaussian (which approximately corresponds to the properties of the histograms of the model’s residual errors for the

processes under consideration), so that the two-dimensional random process (η_1, η_2) is a normal white noise with the covariance matrix Γ . The variances of the processes x_k in (2) are denoted by $\sigma_{x,k}^2$. They may unambiguously be found from the values of the coefficients of model (2) and the matrix Γ . In this case, the model coefficients and the noise variances $\hat{\sigma}_{k|j}^2$ are estimated using the method of least squares, and the noise covariance (nondiagonal element Γ) may be obtained as the corresponding moment estimate from the residual errors of the equations for $k = 1$ and $k = 2$ in (2). One can compare the calculated variances of the processes x_k in constructed model (2) with ordinary moment estimates of the process variances according to observational series (sample variances): for adequate models, they must coincide with an accuracy of statistical error.

The long-term effect $j \rightarrow k$ is estimated using AR model (2) according to the extent to which the observed variance of x_k differs from its values at the zero coupling coefficients $b_{k,i} = 0$ (for all i) in the model and under other equal conditions, in particular, at a constant value of the coupling coefficients $b_{j,i}$ that determine the reverse effect $k \rightarrow j$. The coupling characteristic is denoted by

$$C_{j \rightarrow k} = \frac{\sigma_{x,k}^2 - \sigma_{x,k}^2[b_{k,i} = 0]}{\sigma_{x,k}^2[b_{k,i} = 0]}, \tag{3}$$

where the additional conditions, under which the variance value was obtained, are given in square brackets here and below. The normalization in (3) characterizes the relative difference between the x_k variances for the coupling coefficients $b_{k,i}$ obtained from time series and for the zero coupling $b_{k,i} = 0$. At the unidirectional effect $j \rightarrow k$ (i.e., at zero feedback) and mutually uncorrelated noises, the value of (3) is positive. However, at bidirectional coupling, it may also be negative (see below), so that it is not always possible to interpret this value as a contribution of the process x_j to the variance of x_k .

As a contribution to the variance, one can interpret a similar value obtained under the additional condition of zero values of $b_{j,i}$:

$$C_{j \rightarrow k}^{(0)} = \frac{\sigma_{x,k}^2[b_{j,i} = 0] - \sigma_{x,k}^2[b_{k,i} = 0, b_{j,i} = 0]}{\sigma_{x,k}^2[b_{k,i} = 0, b_{j,i} = 0]}. \tag{4}$$

The value of (4) is always positive (at mutually uncorrelated noises) and it shows to what extent the $b_{k,i}$ values obtained from observational data increase the variance of x_k in model (2) when compared to the case $b_{k,i} = 0$ at zero feedback $b_{j,i} = 0$.

An analysis of variations in the process x_k when the variance σ_{jk}^2 of the noise η_j changes (becomes zero) in the AR equation for the other process (x_j) is close in meaning when compared to its observed value:

$$N_{j \rightarrow k} = \frac{\sigma_{x,k}^2 - \sigma_{x,k}^2 [\sigma_{jk}^2 = 0]}{\sigma_{x,k}^2 [\sigma_{jk}^2 = 0]}. \quad (5)$$

This value is also positive (at mutually uncorrelated noises) even in the case of bidirectional coupling, which makes it possible to use such characteristics for spectral decompositions [32, 33]. At zero feedback $b_{j,i} = 0$, the value of $N_{j \rightarrow k}$ coincides with $C_{j \rightarrow k}^{(0)}$ and $C_{j \rightarrow k}$.

The introduced characteristics reflect the effect of the process x_j on x_k , which involves variations in the stationary (quasi-stationary) characteristic of the process x_k (its variance) under varying parameters. The stationary (quasi-stationary) characteristics empirically manifest themselves in data series whose length significantly exceeds the characteristic time scales of the processes under analysis. Thus, $N_{j \rightarrow k}$, $C_{j \rightarrow k}^{(0)}$, and $C_{j \rightarrow k}$ are the long-term characteristics of the effect.

4. ANALYSIS RESULTS

4.1. Analyzing the Entire 1870–2013 Period

Below, the AMO index corresponds to x_1 and the ENSO index corresponds to x_2 (Fig. 1). An individual model for AMO variations is optimal at $d_1 = 1$: the standard deviation of prediction error is $\sigma_1 = 0.09$ K at the standard deviation $\sigma_{x,1} = 0.21$ K. The individual model for the ENSO is optimal at $d_2 = 6$: $\sigma_2 = 0.29$ K at $\sigma_{x,2} = 0.76$ K. Model (2) for AMO variations with consideration for the ENSO (i.e., the equation with $k = 1$) is optimal at $d_{2 \rightarrow 1} = 2$ with the prediction improvement $PI_{2 \rightarrow 1} = 0.016$ at the significance level $p_{\min} = 3 \times 10^{-6}$; i.e., the ENSO effect on AMO variations is reliably revealed. For the reverse effect, $PI_{1 \rightarrow 2} = 0.002$ at $d_{1 \rightarrow 2} = 1$ with the significance level $p_{\min} = 0.09$; i.e., the AMO effect on the ENSO is less reliably revealed.

When nonlinear models with second-order polynomials are used, they yield almost the same results in simulating AMO variations; however, for ENSO variations, such an analysis yields a smaller value of individual dimensionality ($d_2 = 3$) and probably therefore a further prediction improvement with consideration for the AMO (of an order of 0.01), which is significant at a level of 0.02. However, the Schwartz criterion for nonlinear models proves larger than for linear (both individual and joint) ones, which suggests that the efficiency of the former is lower. A further nonlinear anal-

ysis is efficient; however, in order to obtain reliable results, such an analysis will require additional considerations (for example, the form of nonlinear functions in model and others). In connection with this, the results of only linear analysis are given below.

The long-term effects were estimated on the basis of the abovementioned empirical model

$$\begin{aligned} x_1(t) &= a_{1,1}x_1(t-1) + b_{1,1}x_2(t-1) + b_{1,2}x_2(t-2) + \eta_1(t), \\ x_2(t) &= \sum_{i=1}^6 a_{2,i}x_2(t-i) + b_{2,1}x_1(t-1) + \eta_2(t), \end{aligned} \quad (6)$$

where the noises η_1 and η_2 have the variances $\sigma_1^2 = 0.0071 K^2$ and $\sigma_2^2 = 0.081 K^2$ and the correlation coefficient 0.02 ± 0.02 , $a_{1,1} = 0.91 \pm 0.01$, $b_{1,1} = 0.019 \pm 0.007$, $a_{2,1} = 0.90 \pm 0.02$, $a_{2,2} = 0.14 \pm 0.03$, $a_{2,3} = -0.07 \pm 0.033$, $a_{2,4} = 0.016 \pm 0.033$, $a_{2,5} = -0.024 \pm 0.033$, $a_{2,6} = -0.082 \pm 0.024$, $b_{2,1} = -0.058 \pm 0.034$, (the coefficient values are given with their standard deviations [27]). The variances of x_1 and x_2 in model (6) differ from the corresponding empirical variances by less than 1%, which implies that the model quite adequately reproduces the variances. The characteristics of the long-term effects are as follows: $C_{2 \rightarrow 1} = 0.09$, $C_{1 \rightarrow 2} = 0.001$, $C_{2 \rightarrow 1}^{(0)} = 0.13$, $C_{1 \rightarrow 2}^{(0)} = 0.010$, $N_{2 \rightarrow 1} = 0.13$, and $N_{1 \rightarrow 2} = 0.009$. According to these characteristics, the effect of the ENSO on the AMO is significantly stronger than that of the AMO on the ENSO. The variance of the AMO index noticeably increases (by 9%) due to the ENSO effect when compared to the case without this effect, and when the effect of the AMO on the ENSO is zero, this increase is more significant (13%). It should be noted that the effect $2 \rightarrow 1$ in model (6) decreases the variance of the AMO index x_1 when compared to the case of unidirectional coupling $1 \rightarrow 2$, because the coupling coefficient $1 \rightarrow 2$ (the AMO effect on the ENSO, $b_{1,2}$) is negative and the coupling coefficient $2 \rightarrow 1$ ($b_{2,1}$) is positive. In this case, the characteristics $N_{2 \rightarrow 1}$ and $N_{1 \rightarrow 2}$ almost coincide with $C_{2 \rightarrow 1}^{(0)}$ and $C_{1 \rightarrow 2}^{(0)}$. The presence of the effect of AMO variations on the ENSO causes the variance of the ENSO index σ_2^2 to change by only no more than 1%.

4.2. Analysis by Using Sliding Windows of Different Lengths

Since the interaction between the quasi-cyclic processes under consideration may significantly vary in time, its characteristics were estimated on the basis of models obtained in sliding windows of a fixed length, i.e., within the intervals $[T-W, T]$, where W is the window length and T is the time coordinate of the end of window. For every window the optimal values of model

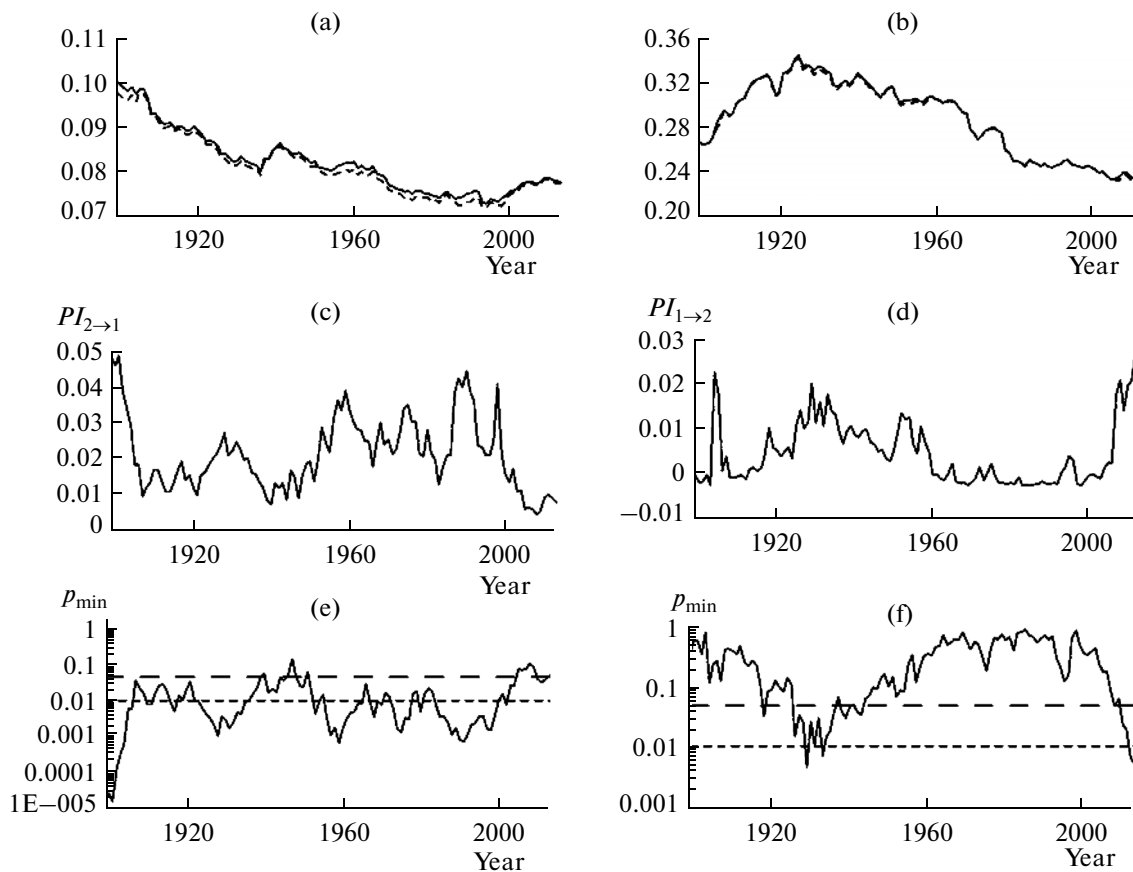


Fig. 2. (a, c, e) Estimates of the short-term effects of ENSO variations on AMO variations and, conversely, (b, d, f) the AMO effects on ENSO variations for a sliding window of 30 years: (a, b) standard deviations of prediction errors for both individual (solid line) and joint (dashed line) AR models, (c, d) estimates of normalized prediction improvements, and (e, f) corresponding values of the significance level of the inference about nonzero prediction improvements according to the F -test for every window (pointwise significance level). Dashed lines correspond to the threshold values: 0.05 (long strokes) and with repeated consideration for the Bonferroni correction (0.05 divided by the number of nonoverlapping windows) (short strokes).

orders were selected using both the Schwartz and Fisher criteria. Such an analysis was made for $W = 30$ years (Figs. 2, 3) and for W increased to 60 years (Figs. 4, 5) and decreased to 20 (Figs. 6, 7) and 10 years.

At $W = 30$ years, the AR model for AMO variations has optimal orders of 1 to 2 (more often 1) for d_1 and 1 to 3 (more often 1) for $d_{2 \rightarrow 1}$. Similarly, for the ENSO, d_2 and $d_{1 \rightarrow 2}$ vary from 1 to 5 (more often 2 or 3 for d_2 and usually 1 for $d_{1 \rightarrow 2}$). Figures 2a and 2b give the standard deviations of prediction errors for both individual and joint AR models (solid and dashed lines, respectively) for both processes: for AMO and ENSO variations, respectively. The relative prediction improvements reach essentially larger values than for the entire interval under analysis (Figs. 2c, 2d), which are significant at both pointwise and general levels (0.05) (see Figs. 2e, 2f). For some window positions, the effect of AMO variations on the ENSO, which is comparable in short-term characteristics to the effect in opposite direction, is revealed: the maximum normalized prediction improvement $PI_{1 \rightarrow 2} > 0.03$ is comparable to the maximum $PI_{2 \rightarrow 1} \approx 0.05$. The influ-

ence of ENSO variations on the AMO for most 30-year intervals is significant (Fig. 2e), and this relation manifest itself as almost unidirectional; however, in the early 21st century, this influence decreases (Figs. 2c, 2e), while the influence of AMO variations on the ENSO has increased in recent years (Figs. 2d, 2f). From the standpoint of the criteria used, this implies the reversal of the direction of influence.

Figure 3 gives estimates of the long-term characteristics of the coupling: (a, b) variances of both processes under different model conditions and (c, d) relative changes in the variances. On the whole, the ENSO effect on the AMO (Fig. 3c) is more intense than the AMO effect on the ENSO: the ENSO effect on the AMO at zero feedback, which is characterized by the value of $C_{2 \rightarrow 1}^{(0)}$ (thick solid line in Fig. 3c), results in a relative increase in the variance of the AMO index up to 40%. The ENSO effect on AMO variations at a fixed feedback, which is characterized by the value of $C_{2 \rightarrow 1}$, does not always result in such a large increase (a thin solid line characterizes the relative difference between the thick and thin solid lines in Fig. 3a), but it

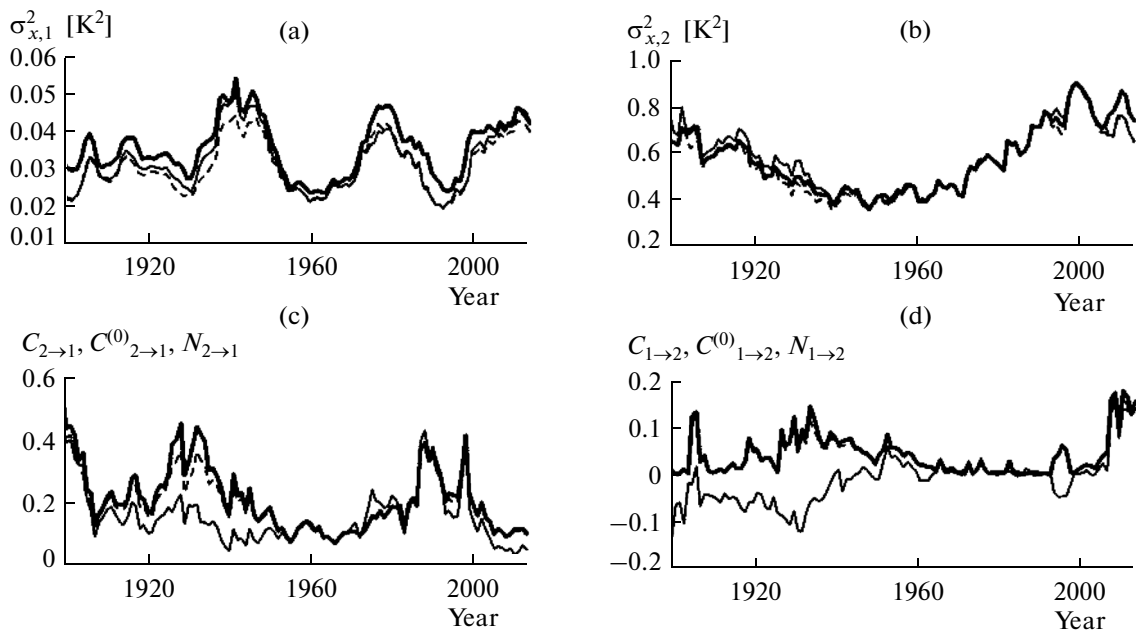


Fig. 3. Estimates of the long-term effects of (a, c) the ENSO on the AMO and (b, d) the AMO on the ENSO for a sliding window of 30 years: (a, b) the variances of the processes x_1 (AMO) and x_2 (ENSO) in model (2) for observed parameter values (thick solid lines), observed parameter values and zero coupling coefficients (a) $b_{1,i}$ or (b) $b_{2,i}$ (thin solid lines), observed parameter values and zero noise levels (a) $\sigma_{2|1}$ or (b) $\sigma_{1|2}$ (thin dashed lines); (c, d) estimates of $C_{j \rightarrow k}^{(0)}$ (4) (thick solid lines), $C_{j \rightarrow k}$ (3) (thin solid lines), and $N_{j \rightarrow k}$ (5) (thin dashed lines).

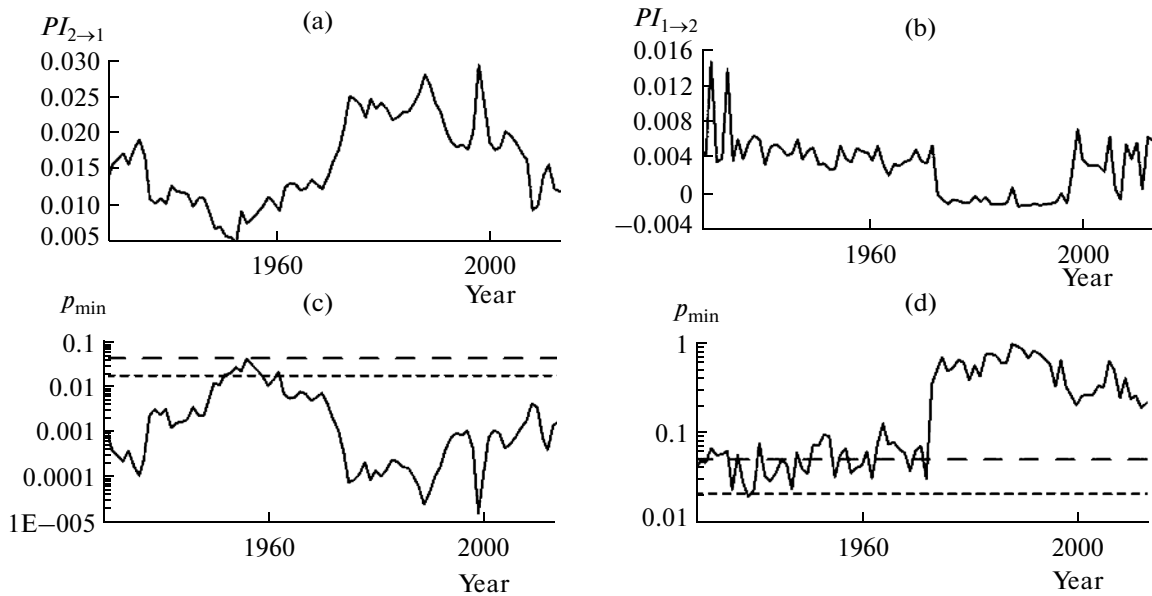


Fig. 4. Estimates of the short-term effects of (a, c) the ENSO on the AMO and (b, d) the AMO on the ENSO for a sliding window of 60 years: (a, b) estimates of normalized prediction improvements and (c, d) corresponding estimates of the significance level. The dashed lines show the threshold values: 0.05 (long strokes) and 0.05 divided by the number of nonoverlapping windows (short strokes).

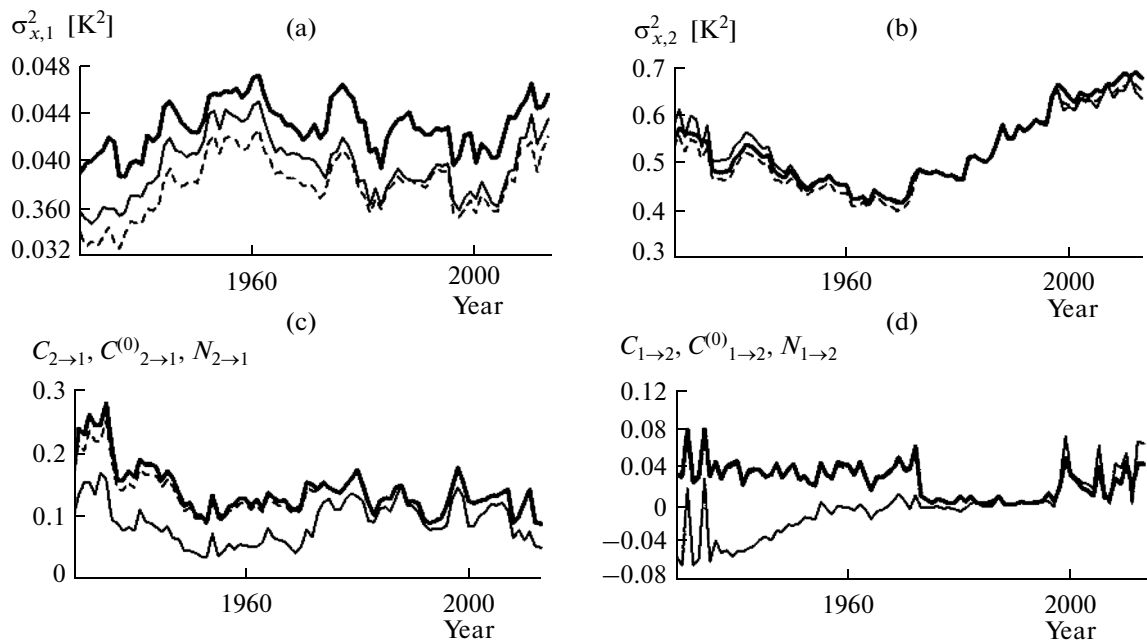


Fig. 5. Estimates of the long-term effects of (a, c) the ENSO on the AMO and (b, d) the AMO on the ENSO for a sliding window of 60 years. Symbols are the same as in Fig. 3.

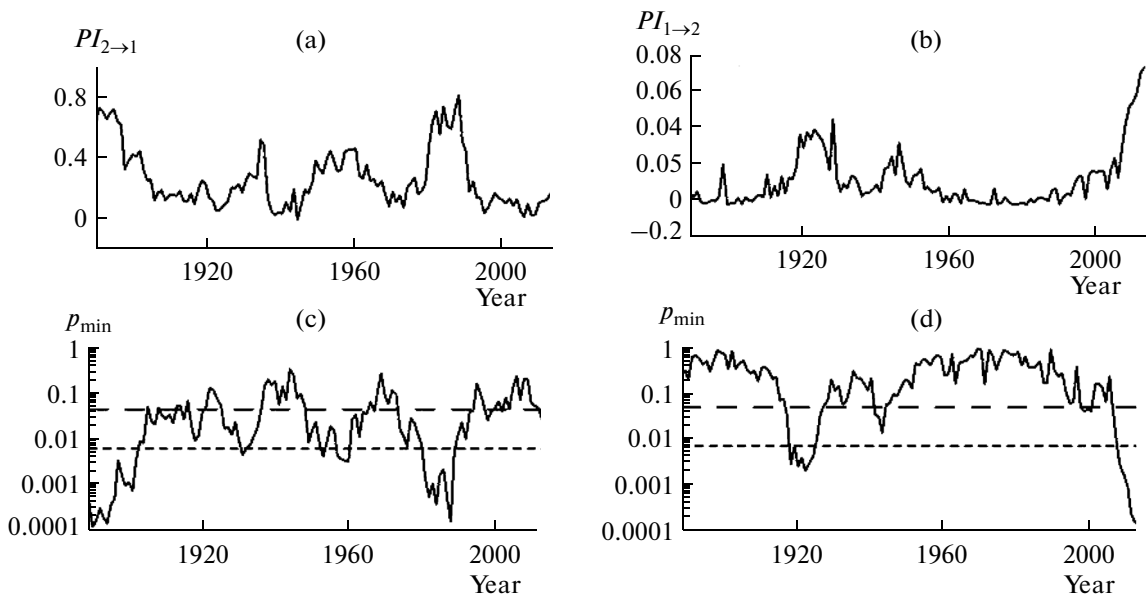


Fig. 6. Estimates of the short-term effects of (a, c) the ENSO on the AMO and (b, d) the AMO on the ENSO for a sliding window of 20 years: (a, b) estimates of normalized prediction improvements and (c, d) corresponding estimates of the significance level. Symbols are the same as in Fig. 4.

is comparable. In the model equation for the ENSO, setting the noise variance $\sigma_{2|1}^2$ equal to its empirical estimate (but not to zero) also increases the variance of the AMO index by 40%. This is represented by the value of $N_{2 \rightarrow 1}$ in Fig. 3a, in which the dashed line characterizes the relative difference between the thick solid

and dashed lines. It should be noted that, in Figs. 3, 5, and 7, the values of $N_{j \rightarrow k}$ are often close to $C_{j \rightarrow k}^{(0)}$ so that the dashed and thick solid lines almost coincide.

On the whole, the effect of AMO variations on the ENSO is not so strong; however, in recent years, this effect has caused the ENSO variance to increase up to

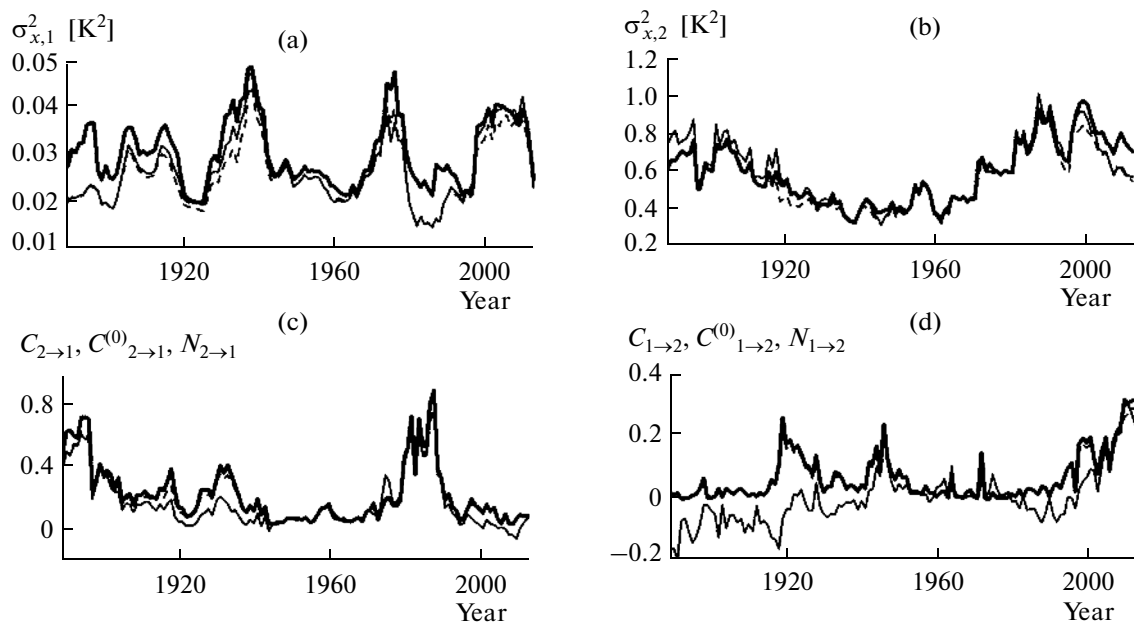


Fig. 7. Estimates of the long-term effects of (a, c) the ENSO on the AMO and (b, d) the AMO on the ENSO for a sliding window of 20 years. Symbols are the same as in Figs 3 and 5.

20% due to the nonzero coefficient of coupling with the AMO (the values of $C_{1 \rightarrow 2}^{(0)}$ and $C_{1 \rightarrow 2}$ reaches approximately the same values. The values of $C_{1 \rightarrow 2}^{(0)}$ and $N_{1 \rightarrow 2}$ reached 10% in earlier periods, for example, in 1901–1930. It should be noted that the $C_{1 \rightarrow 2}$ effect of the variance change due to the nonzero coupling coefficient at a fixed feedback may also be significantly negative (Fig. 3d), which is realized in the presence of effects in both directions with coefficients of different signs. According to the results (Figs. 2, 3), the 1950–1980 period is characterized by insignificant effects in both directions. Before this period, this coupling was bidirectional with the dominating ENSO effect on the AMO and, after this period, almost the unidirectional ENSO \rightarrow AMO coupling was pronounced, which, in recent years, has changed into almost the unidirectional AMO \rightarrow ENSO coupling.

Figures 4 and 5 show similar results obtained using a longer 60-year sliding window. General conclusions are similar, with the difference being that, in the longer window, the effect of AMO variations on the ENSO has not been pronounced in recent years, and only its statistically insignificant features manifest themselves. For shorter 20-year (Figs. 6, 7) and 10-year windows, a more detailed dynamics manifests itself when compared to that for the 30-year window. However, estimates obtained using a 30-year window seem more reliable, because the sampled and calculated (for model (2)) variances of the processes are closer to each other in this window. According to estimates obtained using a 20-year window, the ENSO has the strongest effect on AMO variations also at the beginning of the

period under analysis, and the reverse effect becomes stronger at the end of this period (Figs. 6, 7). It is important that the total length of intervals with significant coupling estimates for a 20-year window significantly decreases when compared to that for a 30-year window. Results obtained using a 10-year window are similar in many aspects, with the difference being that model errors in reproducing signal variances increase still further and intervals of significant coupling estimates are almost absent.

5. CONCLUSIONS

Relatively short-term and longer-term relations between AMO and ENSO variations have been studied using the Granger causality analysis for the former relations. The results of our analysis of data obtained over a period of 1870–2013 suggest that, on the whole, the ENSO effect on the AMO is stronger. The reverse effect is relatively weakly significant and noticeably smaller in value for both short- and long-term couplings. According to estimates for the entire period under analysis, the ENSO increases the variance of AMO-index variations by approximately 10%. The reverse effect for the entire period is, on the whole, weaker by an order of magnitude.

A more detailed analysis with the use of sliding windows (the most informative and reliable results were obtained using a 30-year window) has revealed the time-varying character of these relations. The ENSO effect on the AMO was stronger at the beginning of the period under analysis, and the reverse effect (the AMO effect on the ENSO) has become

more significant and increased in recent years. According to empirical AR models (2), the variance of the AMO index increased to 40% due to the ENSO effect at the beginning of the period under study, and, in recent years, the variance of the ENSO index has increased to 20% due to the AMO effect.

Thus, the results of such an analysis have revealed a bidirectional relation between ENSO and AMO variations with the generally dominating ENSO effect on the AMO. In addition, according to obtained estimates, the AMO effect on the ENSO has increased in recent years, and this tendency for an increase is conserved against the background of a decrease in the ENSO effect on the AMO.

It should be noted that the results presented in this work do not include estimates of the effects of the cross-modulation of both ENSO and AMO cycles. In order to analyze variations in the AMO cycle with a characteristic period of over 50 years, longer series of observational data are necessary. Such an analysis is possible on the basis of data obtained from empirical (paleoclimate) reconstructions and model simulations.

ACKNOWLEDGMENTS

This work was supported by the Russian Foundation for Basic Research (project nos. 14-05-00639 and 14-02-00492), Russian Academy of Sciences programs, and grants from the president of the Russian Federation (NSh-3894.2014.5 and NSh-1726.2014.2) and the Russian government (agreement no. 14.Z50.31.0033 with the Institute of Atmospheric Physics, Russian Academy of Sciences).

REFERENCES

1. *Climate Change 2013: The Physical Science Basis—Contribution of Working Group I to the Fifth Assessment Report of the Intergovernmental Panel on Climate Change*, Ed. by T. F. Stocker, D. Qin, G.-K. Plattner, et al. (Cambridge University Press, Cambridge, 2013).
2. K. Arpe, L. Bengtsson, G. S. Golitsyn, I. I. Mokhov, V. A. Semenov, P. V. Sporyshev, “Analysis and modeling of the hydrological regime variations in the Caspian Sea basin,” *Dokl., Earth Sci.* **366** (4), 552–556 (1999).
3. G. V. Gruza, E. Ya. Ran’kova, L. K. Kleshchenko, and L. N. Aristova, “Coupling between climate anomaly in Russia and ENSO,” *Meteorol. Gidrol.*, No. 5, 32–51 (1999).
4. I. I. Mokhov, A. V. Eliseev, and D. V. Khvorost’yanov, “Evolution of the characteristics of interannual climate variability associated with the El Niño and La Niña phenomena,” *Izv., Atmos. Ocean. Phys.* **36** (6), pp. 681–690 (2000).
5. K. Arpe, L. Bengtsson, G. S. Golitsyn, et al., “Connection between Caspian Sea level variability and ENSO,” *Geophys. Res. Lett.* **27** (17), 2693–2699 (2000).
6. I. I. Mokhov, D. V. Khvorostyanov, and A. V. Eliseev, “Decadal and longer term changes in El Niño—Southern Oscillation characteristics,” *Int. J. Climatol.* **24**, 401–414 (2004).
7. I. I. Mokhov and V. Ch. Khon, “Interannual variability and long-term tendencies of change in atmospheric centers of action in the Northern Hemisphere: Analyses of observational data,” *Izv., Atmos. Ocean. Phys.* **41** (6), 657–666 (2005).
8. I. I. Mokhov, V. A. Semenov, V. Ch. Khon, et al., “Connection between Eurasian and North Atlantic climate anomalies and natural variations in the Atlantic thermohaline circulation based on long-term model calculations,” *Dokl. Earth Sci.* **419** (3), 502–505 (2008).
9. I. I. Mokhov and A. V. Timazhev, “Climatic anomalies in Eurasia from El Niño/La Niña effects,” *Dokl. Earth Sci.* **453** (1), 1141–1144 (2013).
10. C. W. J. Granger, “Investigating causal relations by econometric models and cross-spectral methods,” *Econometrica* **37** (3), 424–438 (1969).
11. C. W. J. Granger, “Testing for causality,” *J. Econ. Dyn. Control* **2**, 329–352 (1980).
12. N. Ancona, D. Marinazzo, and S. Stramaglia, “Radial basis function approach to nonlinear Granger causality of time series,” *Phys. Rev. E* **70** (5), 056221 (2004).
13. D. Marinazzo, M. Pellicoro, and S. Stramaglia, “Kernel method for nonlinear Granger causality,” *Phys. Rev. Lett.* **100**, 144103 (2008).
14. W. Wang, B. T. Anderson, R. K. Kaufmann, and R. B. Myneni, “The relation between the North Atlantic Oscillation and SSTs in the North Atlantic basin,” *J. Clim.* **17** (24), 4752–4759 (2004).
15. T. J. Mosedale, D. B. Stephenson, M. Collins, and T. C. Mills, “Granger causality of coupled climate processes: Ocean feedback on the North Atlantic Oscillation,” *J. Clim.* **19** (7), 1182–1194 (2006).
16. I. I. Mokhov and D. A. Smirnov, “El Niño Southern Oscillation Drives North Atlantic Oscillation as revealed with nonlinear techniques from climatic indices,” *Geophys. Res. Lett.* **33**, L03708 (2006). doi 10.1029/2005GL024557
17. I. I. Mokhov and D. A. Smirnov, “Study of the mutual influence of the El Niño—Southern Oscillation processes and the North Atlantic and Arctic oscillations,” *Izv., Atmos. Ocean. Phys.* **42** (5), 598–614 (2006).
18. I. I. Mokhov and D. A. Smirnov, “Diagnostics of a cause—effect relation between solar activity and the Earth’s global surface temperature,” *Izv., Atmos. Ocean. Phys.* **44** (3), 263–272 (2008).
19. S. S. Kozlenko, I. I. Mokhov, and D. A. Smirnov, “Analysis of the cause and effect relationships between El Niño in the Pacific and its analog in the equatorial Atlantic,” *Izv., Atmos. Ocean. Phys.* **42** (6), 704–713 (2009).
20. E. Kodra, S. Chatterjee, and A. R. Ganguly, “Exploring Granger causality between global average observed time series of carbon dioxide and temperature,” *Theor. Appl. Climatol.* **104**, 325–335 (2011).
21. I. I. Mokhov, D. A. Smirnov, P. I. Nakonechnyi, et al., “Alternating mutual influence of El-Niño/Southern Oscillation and Indian monsoon,” *Geophys. Res. Lett.* **38**, L00F04 (2011). doi 10.1029/2010GL045932
22. I. I. Mokhov, D. A. Smirnov, P. I. Nakonechnyi, et al., “Relationship between El-Niño/Southern Oscillation

- and the Indian monsoon,” *Izv., Atmos. Ocean. Phys.* **48** (1), 47–56 (2012).
23. I. I. Mokhov, D. A. Smirnov, and A. A. Karpenko, “Assessments of the relationship of changes of the global surface air temperature with different natural and anthropogenic factors based on observations,” *Dokl. Earth Sci.* **443** (1), 381–387 (2012).
 24. D. A. Smirnov and I. I. Mokhov, “From Granger causality to long-term causality: Application to climatic data,” *Phys. Rev. E* **80** (1), 016208 (2009).
 25. I. I. Mokhov and D. A. Smirnov, “Empirical estimates of the influence of natural and anthropogenic factors on the global surface temperature,” *Dokl. Earth Sci.* **427** (5), 798–803 (2009).
 26. G. Schwartz, “Estimating the dimension of a model,” *Ann. Stat.* **6** (2), 461–464 (1978).
 27. G. Seber, *Linear Regression Analysis* (Wiley, New York, 1977; Mir, Moscow, 1980).
 28. D. A. Smirnov and B. P. Bezruchko, “Spurious causalities due to low temporal resolution: Towards detection of bidirectional coupling from time series,” *Europhys. Lett.* **100**, 10005 (2012).
 29. D. A. Smirnov and B. P. Bezruchko, “Effect of mutual influence between oscillation systems from observational data,” *Izv. Vyssh. Uchebn. Zaved., Radiofiz.* **55** (10–11), 736–749 (2012).
 30. D. A. Smirnov and I. I. Mokhov, “Estimation of interaction between climatic processes: Effect of sparse sample of analyzed data series,” *Izv., Atmos. Ocean. Phys.* **49** (5), 485–493 (2013).
 31. D. A. Smirnov, “Spurious causalities with transfer entropy,” *Phys. Rev. E* **87** (4), 042917 (2013).
 32. J. Geweke, “Measures of conditional linear dependence and feedback between time series,” *J. Am. Stat. Assoc.* **77**, 304–313 (1982).
 33. M. Dhamala, G. Rangarajan, and M. Ding, “Estimating Granger causality from Fourier and wavelet transforms of time series data,” *Phys. Rev. Lett.* **100** (1), 018701 (2008).

Translated by B. Dribinskaya

SPELL: 1. paleoclimate